PAPER

Ag modified g-C₃N₄ composite entrapped PES UF membrane with visible-light-driven photocatalytic antifouling performance

Manying Zhang, ID * Ziya Liu, Yong Gao and Li Shu

Membrane fouling is still the main obstacle for the wider application of membrane processes. In this study, different amounts of silver modified graphitic carbon nitride (Ag/g-C₃N₄) were firstly introduced into polyethersulfone (PES) membranes by blending *via* a phase-inversion method. The impacts of Ag/g-C₃N₄ addition on the membrane morphology, filtration and photocatalysis antifouling properties of Ag/g-C₃N₄/PES nanocomposite membranes were systematically studied. The results illustrated that the addition of Ag/g-C₃N₄ could make the finger-like voids in Ag/g-C₃N₄ nanocomposite membrane longer and wider, increasing the hydrophilicity and filtration property of the nanocomposite membrane. Also the addition of Ag/g-C₃N₄ nanosheets could endow the nanocomposite membranes with excellent antibacterial, photocatalytic dye degradation and antifouling properties under visible light irradiation.

1. Introduction

Membrane filtration technology has been widely used in many fields due to its reliability and ease of operation. However, membrane fouling remains the main obstacle which strongly restricts its application.[1] According to different pollutants, membrane fouling can be classified into organic fouling, inorganic fouling and biofouling. No matter what kind of fouling occurs, it will result in a significant decline in filtration performance, increased maintenance costs and shortened membrane life.[2] Therefore, many efforts have been made to address this problem.

With the development of nanotechnology, various of nanomaterials have been introduced into polymeric matrices to endow the resulting nanocomposite membranes with desired properties.[2] Silver nanoparticles (AgNPs) have been widely used to modify various of membrane materials by blending or *in situ* reduction, because of their excellent antibacterial property.[3–5] The results showed that the silver based nanocomposite membranes exhibited significant antibacterial and anti-biofouling performances, mainly due to the release of silver ions (Ag⁺).

Nano titanium dioxide (TiO₂) as a traditional photocatalyst also has been widely incorporated into various polymeric materials.[6–8] Many reports indicated that the introduction of TiO₂ could significantly increase the surface hydrophilicity, and improve the ability to degrade organic pollutants by photocatalytic processes.[9,10] Therefore the anti-organic fouling

property can be enhanced. In addition to these merits, the TiO₂ based nanocomposite membrane still faces the challenge of poor photocatalytic performance under visible light irradiation. Besides, most of the current nanomaterial modification strategies are focused on single type of membrane fouling. However, the membrane fouling in the actual process is often very complex and made up of different kinds of membrane fouling. Thus, using a new nanomaterial to address the comprehensive membrane fouling problem has become an urgent need.

Graphitic carbon nitride (g-C₃N₄), which has similar stacked 2D layered structure to graphene, exhibits excellent visible light photocatalysis, chemical and thermal stability.[11,12] It has become the research hot spot in the fields of photocatalysis and environmental purification because of the outstanding photocatalytic property, low cost and simple preparation process. However, the photocatalytic ability of g-C₃N₄ still faces challenge due to the recombination of photo-generated charge carriers.[13,14] In order to remedy this issue, many methods have been taken to modify the pure g-C₃N₄. Among various strategies, noble metal doping as a simple method attracts more attention. Silver nanoparticles (AgNPs) as a popular noble metal were widely used to fabricate Ag/g-C₃N₄ nanocomposite by photodeposition.[12,15,16] Many researchers found the similar phenomenon that the modification of silver nanoparticles could effectively enhanced the photocatalytic activity of g-C₃N₄ due to the improved charge separation efficiency.[12,14]

At present, the modification and application of g-C₃N₄ based materials have been well studied in the field of photocatalysis, but there are few reports in the preparation of organic antifouling membrane materials. Recently, Zhao *et al.* successfully introduced g-C₃N₄/reduced graphene oxide (RGO) on the surface of cellulose acetate (CA) membrane by vacuum

School of Chemical and Environmental Engineering, Jiangsu University of Technology, Changzhou 213001, China. E-mail: myzhang@jsut.edu.cn; Fax: +86 519 86953269; Tel: +86 13616109895

filtration.[17] They found that the addition of g-C$_3$N$_4$/RGO could enhance the degradation ability of organic pollutants and bacterial removal rate of CA composite microfiltration membrane. However, membrane surface modification may araise problems during long time filtration such as the release of particles because of the poor adhesion between photocatalyst and membrane substrate.[18] Alternatively, blending modification is an attractive method due to its facile preparation and stable performance.

As mentioned above, the advantages of Ag/g-C$_3$N$_4$ nanocomposite materials can be summarized as below. First of all, it combines the excellent antibacterial activity of AgNPs and the photocatalytic property of g-C$_3$N$_4$ together. Secondly, the doping of AgNPs by photo-reduction not only can increase the photocatalytic activity of g-C$_3$N$_4$ but also may facilitate the well disperse of AgNPs on the support and decrease the aggregation. Therefore, we considered that the Ag/g-C$_3$N$_4$ composite may be a good alternative that can be used to improve the comprehensive antifouling performance of polymeric membranes.

Thus, in this work Ag/g-C$_3$N$_4$ composite was firstly introduced into polyethersulfone (PES) membranes by blending. The effect of Ag/g-C$_3$N$_4$ composite on membrane morphology, filtration and antibacterial property was studied. Also the photocatalytic performance of nanocomposite membranes was tested by the dye degradation experiment. Furthermore, the influence of inorganic additive on the fouling mitigation capacity of polyethersulfone (PES) membranes under visible light illumination was examined based on the bovine serum albumin (BSA) filtration and by the calculation of flux recovery ratio (FRR) and fouling resistances.

2. Experimental

2.1 Materials

PES (Ultrason E6020P) was purchased from BASF. Melamine (C$_3$H$_6$N$_6$, Analytical grade), silver nitrate (AgNO$_3$), sulfuric acid (H$_2$SO$_4$, analytical grade) and nitric acid (HNO$_3$, analytical grade), N,N-dimethylformamide (DMF) was obtained from Sinopharm Chemical Reagent Co., Ltd. Bovine serum albumin (BSA, 69 kDa), egg albumin (45 kDa), pepsin (35 kDa) were purchased from Sigma Aldrich.

2.2 Preparation and characterization of photocatalyst

In a typical synthesis, 5 g of melamine was heated at 500 °C in a muffle furnace for 2 h and following elevated to the 520 °C with a step of 10 °C min^{-1} for another 2 h for the further reaction. The resultant yellow powder were first dispersed in the mixture of nitric acid (65%) and sulfuric acid (98%) with the volume ratio of 1 : 3, then the turbid liquid was magnetic stirred overnight, the resultant powder was washed by deionized water completely until the neutral and following baked in the oven overnight to get the g-C$_3$N$_4$ nanosheets.

The Ag/g-C$_3$N$_4$ composite photocatalysts were fabricated by photodeposition as described elsewhere.[11,12] Generally, 0.1 g g-C$_3$N$_4$ nanosheets and certain amount of AgNO$_3$ (0.1 mol L^{-1}, 5 mL) was dispersed in 100 mL deionized water with stirring.

Then 10 mL methanol was introduced as sacrificial agent. At last the suspension was irradiated under UV light (11 W, 605 μW cm^{-2}) for 10 h. The Ag/g-C$_3$N$_4$ was obtained after filtration, washing and drying. The final silver concentration was about 140 mg g^{-1} and determined by ICP-OES.

The morphology of obtained samples was characterized by transmission electron microscopy (TEM, Tecnai F30). The crystal structure was examined by X-ray diffraction (XRD, X′ Pert PRO) at a scanning rate of 10° min^{-1} in the range of 10–80°. The chemical structure of the nanocomposite was studied by Fourier transform infrared spectrometer (FTIR) (Thermo Fisher Scientific). Photoluminescence (PL) spectra were studied by a HITACHI spectrometer (F-4600, E_x = 327 nm).

2.3 Preparation of Ag/g-C$_3$N$_4$/PES membranes

All membranes were prepared by the wet phase inversion process. Different amounts of dry Ag/g-C$_3$N$_4$ powders were added into DMF and well dispersed by ultrasonic. Then PES was dissolved and heated at 60 °C until completely dissolved. The dope solution was degassed at 60 °C and then scattered on the nonwoven fabric support with a casting knife gap setting of 200 μm. The nascent membrane was dipped in pure water (25 ± 1 °C) to induce phase inversion. The dope solution was prepared as shown in Table 1.

2.4 Characterization of Ag/g-C$_3$N$_4$/PES membranes

The morphologies of the membranes were observed by SEM (HITACHI S-4800) after coating with gold. The hydrophilicity was evaluated by the contact angle test (CAM200, KSV). The measurements at six different locations were conducted to minimize the error.

The membrane porosity ε(%)of membranes can be estimated as below:

$$\varepsilon = \frac{w_w - w_d}{A \times l \times d_w} \tag{1}$$

The wet weight (w_w) can be obtained after membranes were stored in deionized water for 24 h and dabbing it with filter paper. After 24 h drying at 60 °C, the dry weight (w_d) can be got. A and l are the membrane area (m^2) and thickness (m), respectively. d_w is the water density (0.998 g cm^{-3}).

2.5 Permeate flux measurements

UF experiment was conducted in a dead-end stirred cell at 0.1 MPa. The water flux (J) was obtained with eqn (2)

$$J = \frac{V}{A\Delta t} \tag{2}$$

where V (L) is the volume of permeated water, A (m^2) is the membrane area and Δt (h) is the filtration time.

Molecular weight cut-off (MWCO) is a parameter that reflects the surface pore size of membrane. It can be obtained by the protein rejection (R) calculation of different molecular weight such as BSA (69 kDa), egg albumin (45 kDa), pepsin (35 kDa) and trypsin (24 kDa) with eqn (3)

Table 1 The basic parameters of various membranes

Membrane abbreviation	Silver content (%)	PES (%)	DMF (%)	MWCO (kDa)	CA (°)	Porosity (%)
M0	0	18	82	45	68.5 ± 3.6	70.2
M1	0.1	18	81.9	45	64.5 ± 2.1	71.6
M2	0.3	18	81.7	45	62.0 ± 1.7	74.5
M3	0.5	18	81.5	45	58.9 ± 2.1	79.3
M4	1.00	18	81.00	45	56.4 ± 1.7	81.8

$$R = \left(1 - \frac{C_p}{C_f}\right) \times 100\% \tag{3}$$

where C_p and C_f (g L^{-1}) is the permeate and feed protein concentration, respectively.

2.6 Antibacterial test

The antimicrobial activities of various membranes were firstly tested by agar diffusion method.[19] *Escherichia coli* (*E. Coli*) and *Pseudomonas aeruginosa* (PA) were grown overnight. Then the sterilized membranes were put on the LB agar containing bacteria. After 24 h cultivation, the inhibition ring was recorded by the camera.

The colony forming units counting method was also conducted to characterize the antibacterial effect of various membranes.[20] Briefly, the samples with the same diameter were immersed in the dilute bacterial suspension. After 12 h incubation the number of living bacteria was determined by Colony forming units (CFU) counting.

2.7 Photocatalytic property of membranes

The photocatalytic property of various membranes was tested by the MO degradation experiment. The visible-light was provided by a 300 W xenon lamp with an optical cut-off filter ($\lambda \geq 400$ nm) and the intensity was 100 mW cm^{-2}. First, the membrane (20 cm^2) was anchored to the bottom of the Petri dish using double-sided tape to form a flat membrane surface. Then 50 mL of MO solution (10 mg L^{-1}) was filled in to ensure the fully contact between membrane and dye molecules. The membrane samples were kept 10 cm vertical distance off the visible-light source. During the visible-light illumination, 3 mL solution was collected every 20 min to test the absorption value at 505 nm.

2.8 The antifouling characteristics in photocatalysis

In order to compare the antifouling performance of various membranes, the filtration experiments included four steps were conducted as follows. Firstly, the pure water flux (J_{w1}) was recorded for 0.5 h. Then the BSA solution (1 g L^{-1}) was fed in the cell and the flux (J_p) was recorded for 0.5 h. The fouled membranes were cleaned by deionized water and the third water flux (J_{rw}) was measured for another 0.5 h. Finally, in order to prove the photocatalysis antifouling property of nano-composite membrane, the BSA fouled membrane was irradiated by the xenon lamp for 1 h and the flux (J_{w2}) were recorded again

for 0.5 h in order to get the flux recovery ratio. The FRR before and after visible light irradiation can be got using eqn (4).

$$FRR = \left(\frac{J_{w2}}{J_{w1}}\right) \times 100\% \tag{4}$$

Moreover, the fouling resistance parameters were analyzed to study the fouling process. The irreversible (R_{ir}), reversible (R_r) and total fouling ratio (R_t) were calculated as:

$$R_t = \left(1 - \frac{J_p}{J_{w1}}\right) \times 100 \tag{5}$$

$$R_r = \left(\frac{J_{w2} - J_p}{J_{w1}}\right) \times 100 \tag{6}$$

$$R_{ir} = \left(\frac{J_{w1} - J_{w2}}{J_{w1}}\right) \times 100 \tag{7}$$

3. Results and discussion

3.1 The morphology of photocatalyst

TEM was used to observe the morphology of nanocomposite. Fig. 1a shows a typical rippled 2D paper-like flat layered structure of pure g-C$_3$N$_4$, which is consistent with reported results.[12,16] From Fig. 1b it was clearly observed that a number of silver nanoparticles were well dispersed on the g-C$_3$N$_4$ sheet without obvious aggregation for composite material.

The XRD pattern of nanocomposite is shown in Fig. 2. The peaks at 12.8° and 27.1° of pure g-C$_3$N$_4$ are attributed to the in-plane structure packing of tristriazine units and interlayer-stacking reflection respectively.[12,21,22] As for the Ag/g-C$_3$N$_4$ sample, the diffraction peaks at 38.1° and 44.2° were observed which are indexed to the (111) and (200) planes of silver.[12]

The chemical structure of samples was further characterized by FTIR. Fig. 3 shows the typical molecular structure of g-C$_3$N$_4$. The broad peak at 3000–3500 cm^{-1} is attributed to the N–H stretching vibration.[12,23] The peak at 808 cm^{-1} may be attributed to the triazine units breathing.[24,25] The multiple peaks in the 1200–1700 cm^{-1} region, with the characteristic peaks at and 1240 and 1652 cm^{-1}, may be assigned to the stretching vibration of CN heterocycles.[22,25] The Ag/g-C$_3$N$_4$ sample shows the similar spectra, illustrating the doping of silver did not change the original chemical structure of g-C$_3$N$_4$ which was in accordance with the early reports.[12]
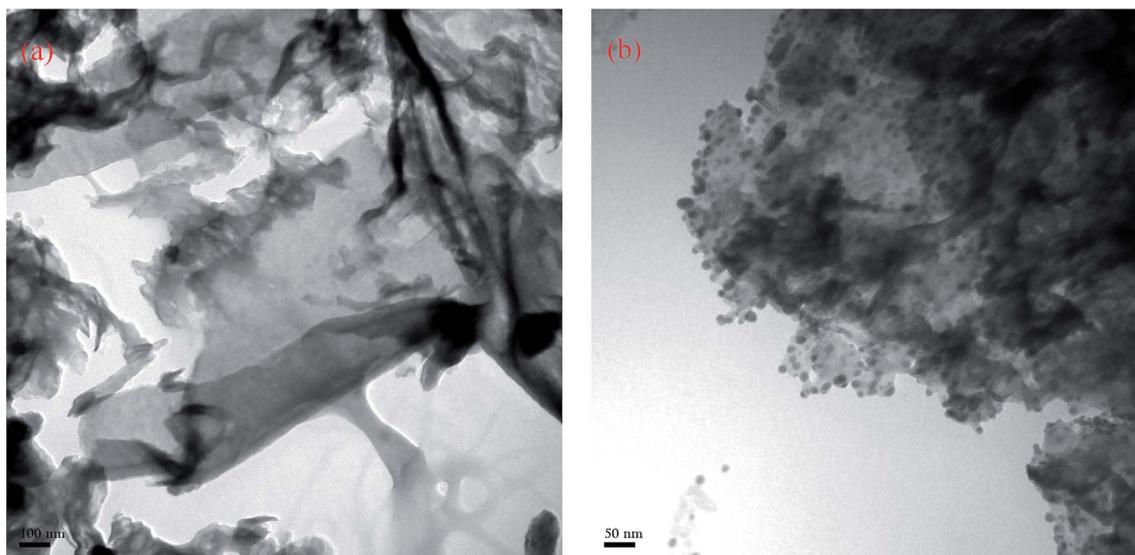
Fig. 1 TEM morphology of (a) pure g-C$_3$N$_4$ nanosheet and (b) Ag/g-C$_3$N$_4$ composites.
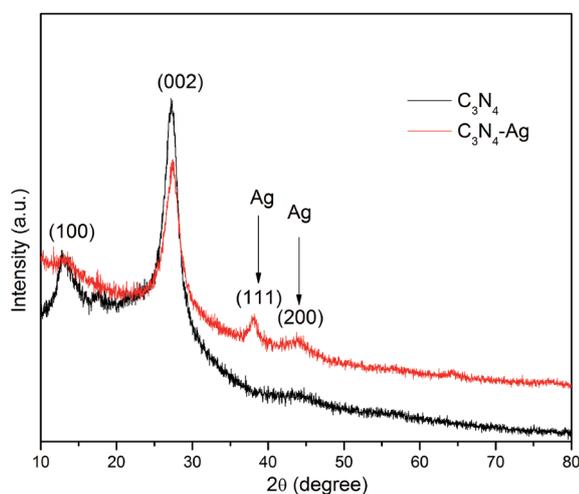
Fig. 2 XRD patterns of the g-C$_3$N$_4$ and Ag/g-C$_3$N$_4$ composite.

increase of Ag/g-C$_3$N$_4$ content, some white particles were observed on the nanocomposite membrane surfaces, which may be the aggregates of Ag/g-C$_3$N$_4$ nanosheets. The overall surface morphologies of nanocomposite membranes were still flat and smooth, indicating that the addition of Ag/g-C$_3$N$_4$ has little effects on surface structure.

Fig. 5b exhibits all the membranes own the dense selective layer, thicker finger-like layer and sponge like pores at the bottom which is the typical asymmetric structure. Compared to M0, the finger-like voids in Ag/g-C$_3$N$_4$ modified membrane become longer and wider. This effect becomes more pronounced with the further increased Ag/g-C$_3$N$_4$ loading. As for M2, M3 and M4 the finger-like voids almost elongate across the whole cross section, also there are macropores formed at the bottom of M4, which are beneficial for the increased water flux. It is considered that the relative diffusion rate and driving force
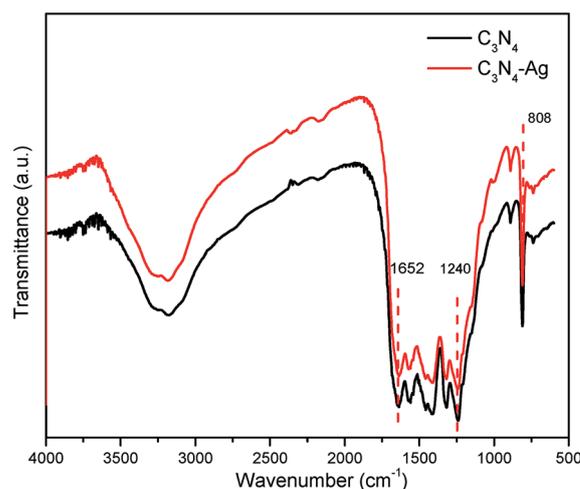
PL spectra is a widely used method to study the photochemical behavior of photocatalyst. Fig. 4 showed that the emission peaks of samples centered at about 470 nm. The PL intensity of composite material reduced significantly compared to the g-C$_3$N$_4$. It is reported that the PL emission derives from the recombination of photo induced electron/hole pairs.[12] The weaker intensity represents the lower recombination rate of free charge carriers.[26] Therefore, the dispersion of Ag in the matrix of g-C$_3$N$_4$ could promote the charge separation, subsequently increasing the photocatalytic activity.[12] The results above indicating that the use of Ag/g-C$_3$N$_4$ composite for the modification of the organic membrane is a meaningful attempt.

3.2 Characterization of membranes

3.2.1 Membrane morphology. As shown in Fig. 5a, pure PES membrane (M0) has a smooth and clean surface. With the

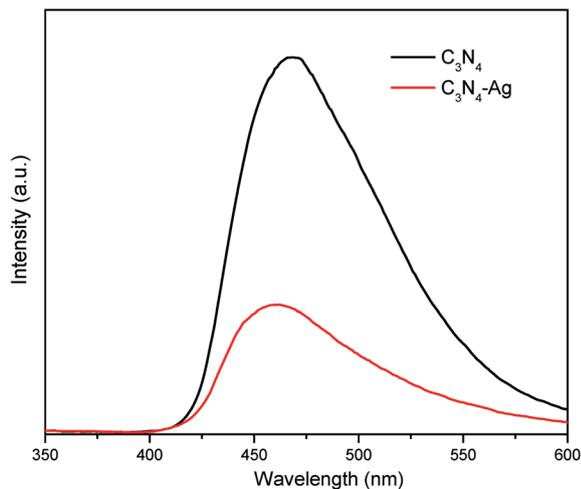**Fig. 3** The FTIR characterization of the g-C$_3$N$_4$ and Ag/g-C$_3$N$_4$ composite.

Fig. 4 PL spectra of pure g-C_3N_4 and Ag/g-C_3N_4 composite.

have great influences on membrane structure.[27] The presence of Ag/g-C_3N_4 nanosheets may enhance the instability of casting solution and induce the accelerated demixing process. The accelerated demixing process may facilitate the fully development of the finger-like micro voids in nanocomposite membranes.[28] It is also believed that if the nanoparticles had higher affinity to non-solvent, elongated macrovoids could appear due to the higher solvent/non-solvent exchange rate.[29] In this study, the hydrophilic group such as –NH as shown in Fig. 3 and the highly dispersed hydrophilic silver nanoparticles on g-C_3N_4 nanosheets may facilitate the exchange rate of solvent and non-solvent. Hence, the macrovoids formed at the bottom of the composite membranes (M4) due to the presence of large amount of Ag/g-C_3N_4 nanosheets.

3.2.2 Hydrophilicity, porosity and pore size of various membranes. The contact angles were used to evaluate the surface hydrophilicity (Table 1). The contact angle of M0 was 68.5°, which was consistent with previous results.[20] The overall contact angle reduced with the incorporation of Ag/g-C_3N_4, which revealed that the hydrophilicity of membrane was increased by Ag/g-C_3N_4. The existence of hydrophilic groups such as –NH_2 or –NH after treated by sulfuric acid and nitric acid and the high affinity of Ag to water may be responsible for the hydrophilicity increase.[12,18] This is also confirmed by FTIR results as shown in Fig. 3.

The overall porosity of various membranes is shown in Table 1. A slightly increased porosity can be observed for Ag/g-C_3N_4 modified membranes. This is consistent with the cross-section pore structure change. As presented in Fig. 5b, wider and prolonged finger-like voids were formed due to the introduction of Ag/g-C_3N_4 nanosheets may lead to the increased porosity.

Molecular weight cut-off (MWCO) is an important parameter to reflect the UF membrane pore size. As shown in Table 1, all the membranes have the same MWCO of 45 kDa indicating that the additions of Ag/g-C_3N_4 nanosheets do not significantly change the surface membrane pore size.

3.3 The permeation and rejection properties

Dead-end filtration was performed to study the filtration performance of various samples as shown in Fig. 6. Compared to M0, the flux of nanocomposite membranes kept increasing and M4 had the highest flux of 268 L m^{-2} h^{-1}. Considering all the membranes have the same MWCO, the changes in flux with the incorporation of Ag/g-C_3N_4 may be clarified as below. Firstly, the incorporation of g-C_3N_4 improved the hydrophilicity and the porosity of nanocomposite membranes which may further improve the water uptake property. Secondly, the introduction of Ag/g-C_3N_4 enlarged the finger-like pore and improved the inter-connectivity of cross section pore structure, which reduced the hydraulic resistance and enhanced the flux permeate. The flux change was consistent with the variation of pore structure, porosity and hydrophilicity of membrane surfaces.

The BSA rejection of various membranes was 94.2%, 96.5%, 96.1%, 95.3%, 94.9%, respectively. The small differences in BSA rejection were attributed to the same MWCO of various membranes. The results indicated that the blending of Ag/g-C_3N_4 may be an effective way to promote the water flux without sacrifice of BSA rejection.

3.4 Antibacterial properties of membranes

The inhibition zone is a simple and widely used method to characterize the inactivation activity of membranes.[30] As shown in Fig. 7, no bactericidal effect was observed for virgin PES (M0). All the modified membranes presented clear and wide inhibition zone and the width of inhibition zone was proportional to the Ag/g-C_3N_4 content, indicating the significant inactivation efficiency towards *P. aeruginosa* and *E. coli*.

Moreover, the results of colony forming units counting also verified the inactivation efficiency. As shown in Table 2, the control (without membrane) and M0 had the maximal values of log CFU. The exists of Ag/g-C_3N_4 modified membranes significantly decrease the number of live bacteria. Specifically for M3 and M4, no living bacteria were found in the test indicating the excellent bactericidal effect of nanocomposite membranes.

The results above clearly revealed that the modification of Ag/g-C_3N_4 could endow the PES membrane with outstanding antibacterial performance. It was reported that the silver based nanocomposite membranes could release silver ions (Ag$^+$) to the surrounding.[19] Ag$^+$ can induce the serious destruction of cell membrane and proteins, which may be one of the main sources of excellent antimicrobial properties of nanocomposite membranes.[3,4]

3.5 Photocatalytic property of membranes

Methyl orange (MO) is a widely used organic dye. As reference, the visible-light photodegradation property of pure PES membrane (M0) was also investigated under the same condition. As shown in Fig. 8, almost no photo degradation effect of MO was observed for M0. This indicated that PES and nonwoven fabric didn't show any photocatalytic performance. In contrast, the introduction of Ag/g-C_3N_4 could enhance the
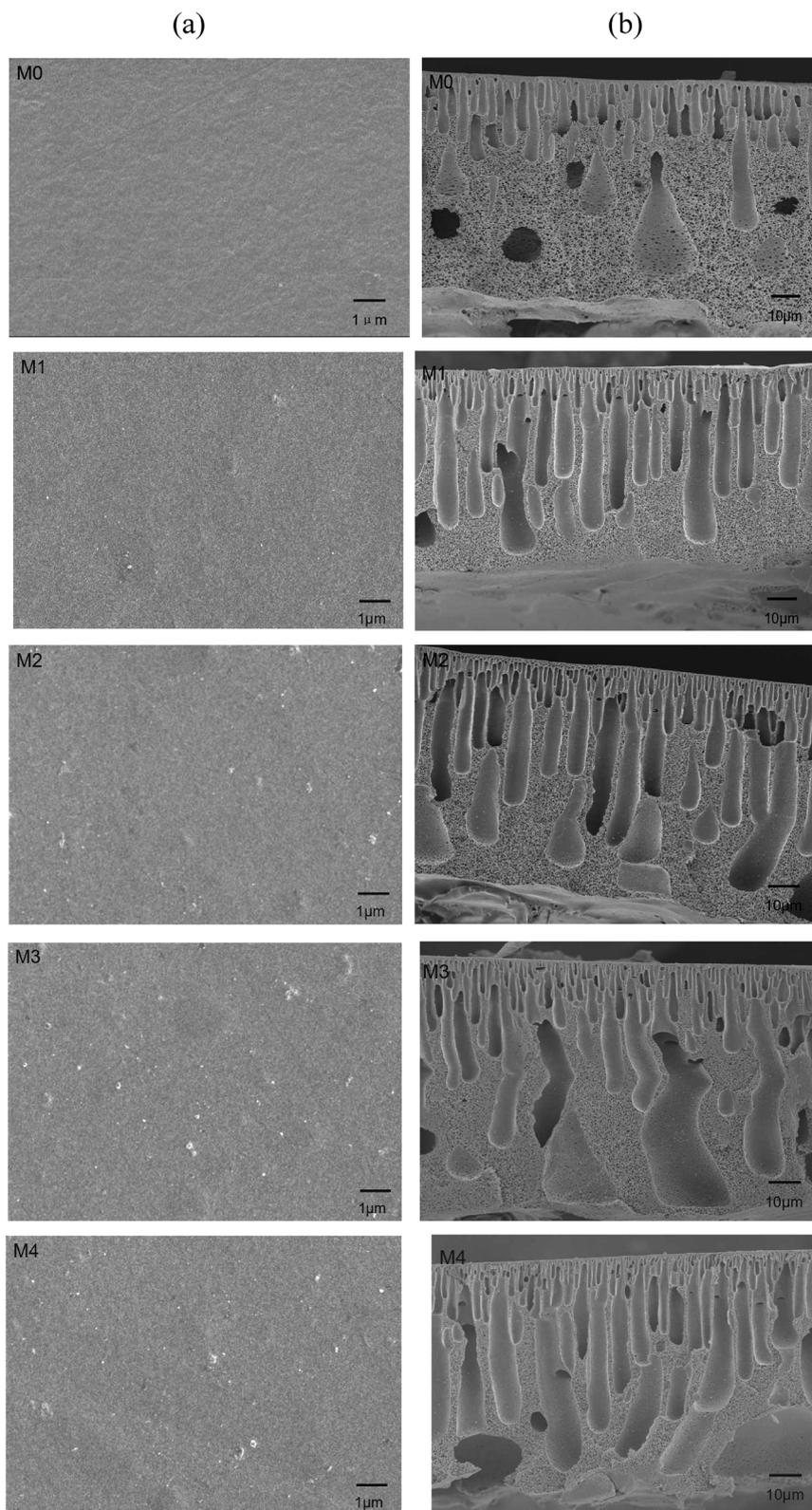
(a)   (b)

Fig. 5 The SEM morphologies of membranes. (a) Surface, (b) cross section.

photocatalytic activity of nanocomposite membranes under visible-light. The M2 owned 66% degradation efficiency toward MO. While the degradation activity kept improving with the increase of Ag/g-C_3N_4 content. As for M4, the degradation efficiency was up to 77%. The results above confirmed that the incorporation of Ag/g-C_3N_4 could significantly increase the
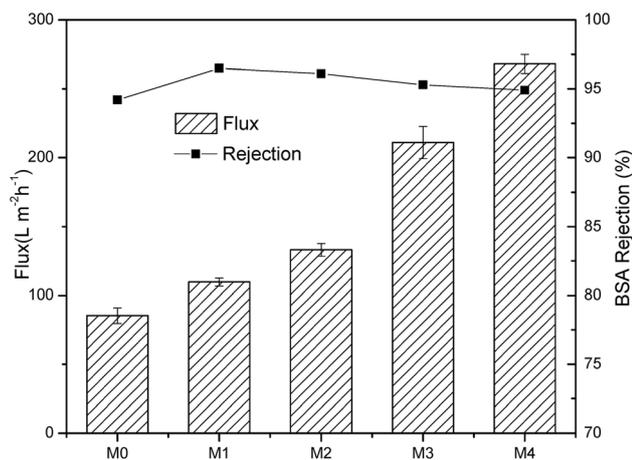
Fig. 6   The pure water flux and BSA rejection of various membranes.

Table 2 Bacteriostatic effects of various membranes on *Escherichia coli* and *Pseudomonas aeruginosa*[a]

Membrane no.	PA (log CFU)	EC (log CFU)
Control	10.78 ± 0.04	9.64 ± 0.07
M0	10.54 ± 0.08	9.50 ± 0.1
M1	4.53 ± 0.11	3.63 ± 0.06
M2	—	2.91 ± 0.09
M3	—	—
M4	—	—

[a] —: no found.

photocatalytic property of nanocomposite membrane under visible-light illumination.

The possible degradation mechanism under visible-light was mainly attributed to the generation of photo-electrons (e^-) and holes (h^+) by g-C_3N_4. The photo-electrons (e^-) could react with the oxygen molecule (O_2) to produce superoxide radical anion $O_2{}^{\bullet-}$. Meanwhile the Ag nanoparticles could entrap the e^- to prevent the recombination of e^- and h^+, thus improving the transfer of charge carriers. The enriched holes and $O_2{}^{\bullet-}$ are responsible for the degradation of Methyl orange (MO).[6,17,31]

3.6   The antifouling performance in photocatalysis

To study the alleviative effect of photocatalysis on membrane fouling, the BSA filtration tests were conducted. As shown in Fig. 9, the water flux declined sharply during BSA filtration step, which is attributed to the deposition of BSA and the formation of cake layers on membrane surfaces. Nevertheless, the Ag/g-
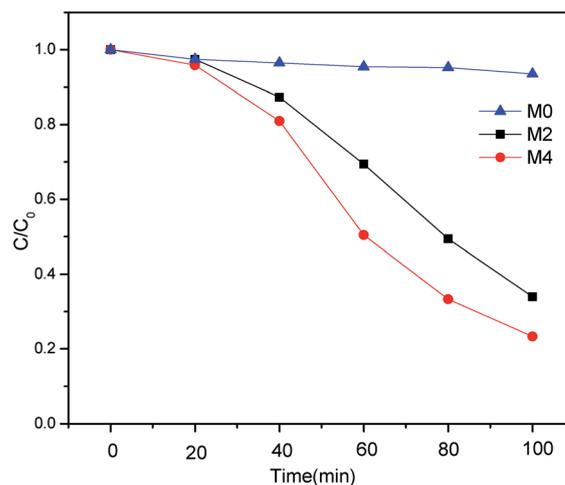

Fig. 8   Degradation rate of MO under visible light irradiation for various membranes.

C_3N_4 modified membranes owned higher fluxes compared to M0. After simple water rinsing, the fluxes of all samples enhanced in different degrees, indicating that the loosely
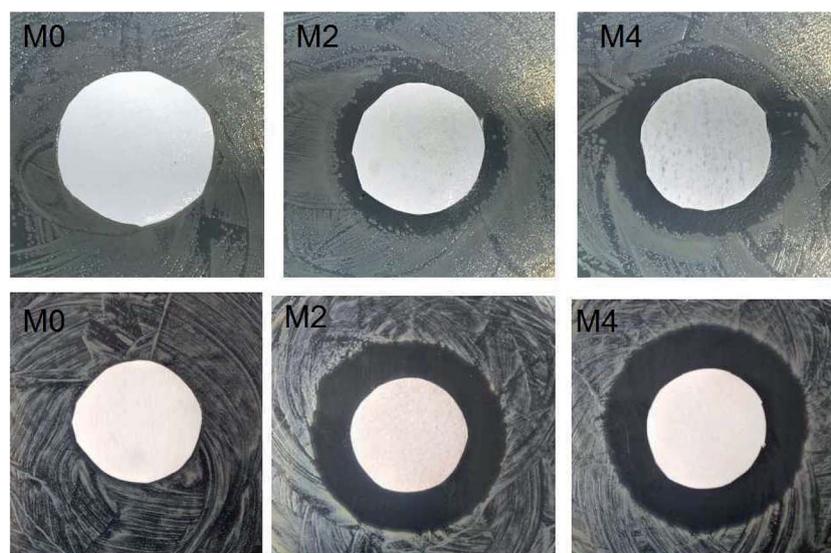

Fig. 7   The antibacterial effect of nanocomposite membranes on (a) *Escherichia coli* (b) *Pseudomonas aeruginosa* observed in the disk diffusion test.
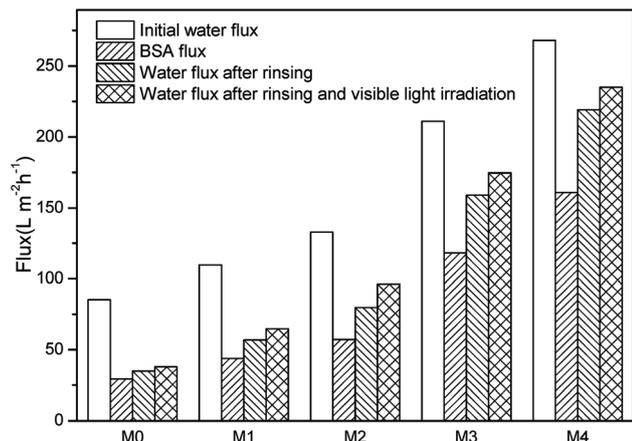
Fig. 9 The flux values of various membranes at different processes.

bound BSA and the cake layer can be removed by hydraulic shear force.

Flux recovery ratio (FRR) is an important parameter to characterize the antifouling property of membranes and it is generally believed that the higher FRR means better antifouling performance.[32,33] As shown in Fig. 10, the FRR of M0 was as low as 41% and all composite membranes had higher FRR than pristine PES membrane (without light). The modification of Ag/g-C$_3$N$_4$ significantly increased the FRR of nanocomposite membranes and M4 owned the maximum FRR (81.7%) without visible-light irradiation. The improved hydrophilicity of membrane surface (Table 1) compared to M0 may contribute to the promoted antifouling behavior. After the supplementation of visible light illumination following water rinsing, further flux increase was observed for nanocomposite membranes (Fig. 9) and the FRR reached to 59.1%, 72.2%, 82.7% and 87.7% respectively (Fig. 10). But as for M0, the further flux increment was less than that of composite membranes. The further recovery of flux and FRR indicated the photocatalytic degradation of strongly bound organic pollutants, which was similar with the results before.[32,33]

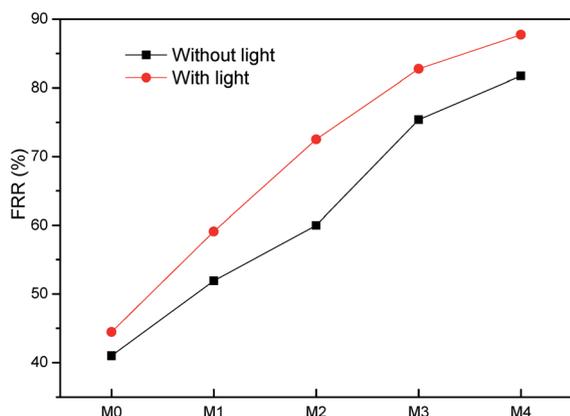To further investigate the membrane fouling details, different fouling ratio were calculated. The R_r and R_{ir} were mainly related to loosely bound protein on membrane surface and the plugging of protein in membrane pores, respectively.[33]

As shown in Fig. 11, all the Ag/g-C$_3$N$_4$ modified membranes had obvious lower R_t than M0, which may be explained by the increase of surface hydrophilicity. The initial R_r values after water rinsing of various samples were 6.5%, 11.8%, 16.9%, 19.4% and 21.7% respectively. After the visible light illumination, the R_r value of Ag/g-C$_3$N$_4$ modified membranes increased to 19.1%, 29.1%, 26.7% and 27.7%, respectively.

Moreover, the ratio of R_{ir} and R_r to the R_t was also calculated. As shown in Fig. 12, the R_r/R_t was 9.9%, 19.8%, 29.7%, 44.0% and 54.3% for various samples without visible light illumination. While the R_r/R_t values increased to 15.3%, 31.8%, 51.2%, 60.8% and 69.3% under visible light irradiation, respectively. This trend showed that reversible fouling (R_r) gradually became the dominant fouling factor with the increase of nanocomposite loading. Fig. 10–12 were consistent with each other, indicating the improved antifouling performance of membranes with the addition of Ag/g-C$_3$N$_4$.
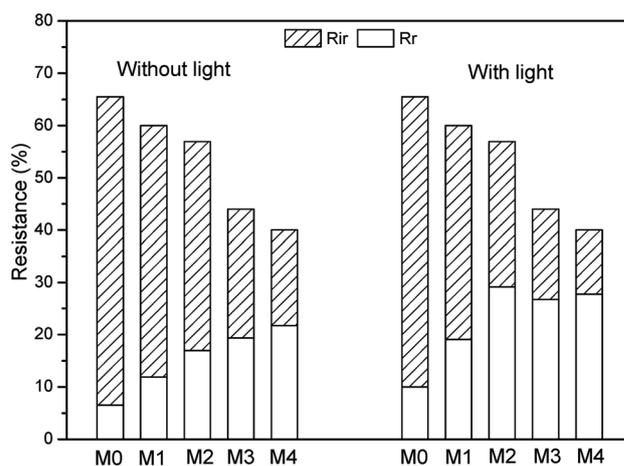

Fig. 11 The distribution of fouling resistance of all the membranes.

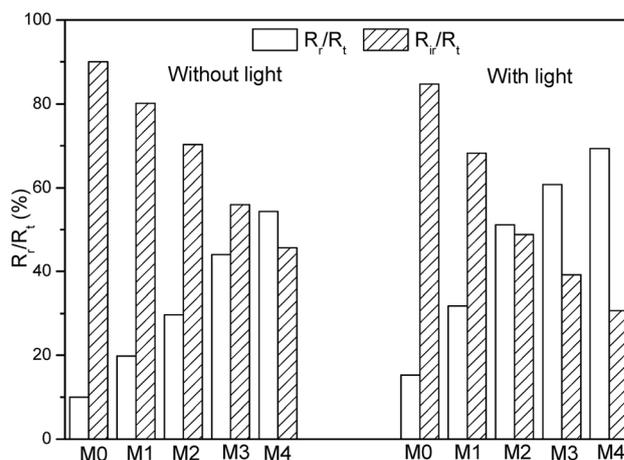Fig. 10 The flux recovery ratio (FRR) of membranes before and after visible light irradiation.

Fig. 12 The ratio of irreversible fouling (R_{ir}) and reversible fouling (R_r) to the total fouling (R_t).

As mentioned above, the enriched holes and $O_2^{\cdot-}$ that generated by g-C_3N_4 under visible light irradiation can degrade many kinds of complex organic materials.[34,35] All the results above confirmed that the holes and $O_2^{\cdot-}$ can induce the degradation of strongly bound pollutants and make the pollutants more easier to be removed from membrane surface, thus decreasing the R_{ir} and improving the photocatalytic anti-fouling property of nanocomposite membranes.

4. Conclusions

In this study, a novel Ag/g-C_3N_4/PES ultrafiltration membrane was successfully fabricated by phase-inversion method. The incorporation of Ag/g-C_3N_4 into PES membranes as additives was systematically studied. The SEM pictures illustrated that the addition of Ag/g-C_3N_4 could make the finger-like voids in Ag/g-C_3N_4 nanocomposite membranes longer and wider. The membrane hydrophilicity and porosity were slightly enhanced due to the introduction of Ag/g-C_3N_4 nanosheets. The bacterial tests showed the excellent antibacterial property of Ag/g-C_3N_4 based nanocomposite membranes. The dye degradation experiments confirmed the significantly improved photo-catalytic effect of nanocomposite membrane by the incorporation of Ag/g-C_3N_4 nanosheets with visible light illumination. The BSA filtration experiments indicated the introduction of Ag/g-C_3N_4 can endow PES membrane with photocatalytic self-cleaning property and improve the antifouling performance. The work may contribute to a potential research of the Ag/g-C_3N_4 in advanced membrane materials. All advantages shown by the Ag/g-C_3N_4/PES nanocomposite membrane make it promising for wider industrial application.

Conflicts of interest

There are no conflicts to declare.

Acknowledgements

References

1 C. S. Ong, P. S. Goh, W. J. Lau, N. Misdan and A. F. Ismail, Nanomaterials for biofouling and scaling mitigation of thin film composite membrane: A review, *Desalination*, 2016, **393**, 2–15.

2 Q. Yang and B. Mi, Nanomaterials for Membrane Fouling Control: Accomplishments and Challenges, *Adv. Chron. Kidney. Dis.*, 2013, **20**, 536–555.

3 L. F. Dumée, L. He, P. C. King, M. L. Moing, I. Güller, M. Duke, P. D. Hodgson, S. Gray, A. J. Poole and L. Kong, Towards integrated anti-microbial capabilities: Novel bio-fouling resistant membranes by high velocity embedment of silver particles, *J. Membr. Sci.*, 2015, **475**, 552–561.

4 M. Sile-Yuksel, B. Tas, D. Y. Koseoglu-Imer and I. Koyuncu, Effect of silver nanoparticle (AgNP) location in nanocomposite membrane matrix fabricated with different polymer type on antibacterial mechanism, *Desalination*, 2014, **347**, 120–130.

5 M. Ben-Sasson, X. Lu, E. Bar-Zeev, K. R. Zodrow, S. Nejati, G. Qi, E. P. Giannelis and M. Elimelech, In situ formation of silver nanoparticles on thin-film composite reverse osmosis membranes for biofouling mitigation, *Water Res.*, 2014, **62**, 260–270.

6 Y. Zhang and M. Cui, Porous YxFeyZr1−x−yO₂ coated TiO₂ solid superacid particles/PVDF hybrid membranes with anti-fouling property, *Chem. Eng. J.*, 2016, **301**, 342–352.

7 M. Safarpour, V. Vatanpour and A. Khataee, Preparation and characterization of graphene oxide/TiO₂ blended PES nanofiltration membrane with improved antifouling and separation performance, *Desalination*, 2016, **393**, 65–78.

8 N. A. M. Nor, J. Jaafar, A. F. Ismail, M. A. Mohamed, M. A. Rahman, M. H. D. Othman, W. J. Lau and N. Yusof, Preparation and performance of PVDF-based nanocomposite membrane consisting of TiO₂ nanofibers for organic pollutant decomposition in wastewater under UV irradiation, *Desalination*, 2016, **391**, 89–97.

9 Y. Zhang and J. Zhu, Composite photocatalytic membrane prepared by embedding porous SiO₂ shell/void/TiO₂ core particles into polycarbonate for photodegrading and removing pollutant from water, *Chem. Eng. Sci.*, 2015, **126**, 390–398.

10 J. P. Méricq, J. Mendret, S. Brosillon and C. Faur, High performance PVDF-TiO₂ membranes for water treatment, *Chem. Eng. Sci.*, 2015, **123**, 283–291.

11 Z. Zhu, X. Tang, C. Ma, M. Song, N. Gao, Y. Wang, P. Huo, Z. Lu and Y. Yan, Fabrication of conductive and high-dispersed Ppy@Ag/g-C₃N₄ composite photocatalysts for removing various pollutants in water, *Appl. Surf. Sci.*, 2016, **387**, 366–374.

12 W. Zhang, L. Zhou and H. Deng, Ag modified g-C₃N₄ composites with enhanced visible-light photocatalytic activity for diclofenac degradation, *J. Mol. Catal. A: Chem.*, 2016, **423**, 270–276.

13 M. Zhang, W. Luo, Z. Wei, W. Jiang, D. Liu and Y. Zhu, Separation free C₃N₄/SiO₂ hybrid hydrogels as high active photocatalysts for TOC removal, *Appl. Catal., B*, 2016, **194**, 105–110.

14 G. Mamba and A. K. Mishra, Graphitic carbon nitride (g-C₃N₄) nanocomposites: A new and exciting generation of visible light driven photocatalysts for environmental pollution remediation, *Appl. Catal., B*, 2016, **198**, 347–377.

15 M. J. Muñoz-Batista, O. Fontelles-Carceller, M. Ferrer, M. Fernández-García and A. Kubacka, Disinfection capability of Ag/g-C3N4 composite photocatalysts under UV and visible light illumination, *Appl. Catal., B*, 2016, **183**, 86–95.

16 S. Ma, S. Zhan, Y. Jia, Q. Shi and Q. Zhou, Enhanced disinfection application of Ag-modified g-C3N4 composite under visible light, *Appl. Catal., B*, 2016, **186**, 77–87.

17 H. Zhao, S. Chen, X. Quan, H. Yu and H. Zhao, Integration of microfiltration and visible-light-driven photocatalysis on g-C_3N_4 nanosheet/reduced graphene oxide membrane for enhanced water treatment, *Appl. Catal., B*, 2016, **194**, 134–140.

18 M. Zhang, R. W. Field and K. Zhang, Biogenic silver nanocomposite polyethersulfone UF membranes with antifouling properties, *J. Membr. Sci.*, 2014, **471**, 274–284.

19 S. Liu, M. Zhang, F. Fang, L. Cui, J. Wu, R. Field and K. Zhang, Biogenic silver nanocomposite TFC nanofiltration membrane with antifouling properties, *Desalin. Water Treat.*, 2015, 1–12.

20 M. Zhang, K. Zhang, B. De Gusseme and W. Verstraete, Biogenic silver nanoparticles (bio-Ag^0) decrease biofouling of bio-Ag^0/PES nanocomposite membranes, *Water Res.*, 2012, **46**, 2077–2087.

21 L. C. Chen, X. T. Zeng, P. Si, Y. M. Chen, Y. W. Chi, D. H. Kim and G. N. Chen, Gold Nanoparticle-Graphite-Like C_3N_4 Nanosheet Nanohybrids Used for Electrochemiluminescent Immunosensor, *Anal. Chem.*, 2014, **86**, 4188–4195.

22 L. Liu, Y. Qi, J. Lu, S. Lin, W. An, Y. Liang and W. Cui, A stable Ag_3PO_4@g-C_3N_4 hybrid core@shell composite with enhanced visible light photocatalytic degradation, *Appl. Catal., B*, 2016, **183**, 133–141.

23 M. Faisal, A. A. Ismail, F. A. Harraz, S. A. Al-Sayari, A. M. El-Toni and M. S. Al-Assiri, Synthesis of highly dispersed silver doped g-C_3N_4 nanocomposites with enhanced visible-light photocatalytic activity, *Mater. Des.*, 2016, **98**, 223–230.

24 Y. Shi, S. Jiang, K. Zhou, C. Bao, B. Yu, X. Qian, B. Wang, N. Hong, P. Wen, Z. Gui, Y. Hu and R. K. K. Yuen, Influence of g-C_3N_4 Nanosheets on Thermal Stability and Mechanical Properties of Biopolymer Electrolyte Nanocomposite Films: A Novel Investigation, *ACS Appl. Mater. Interfaces*, 2013, **6**, 429–437.

25 S. C. Yan, Z. S. Li and Z. G. Zou, Photodegradation Performance of g-C_3N_4 Fabricated by Directly Heating Melamine, *Langmuir*, 2009, **25**, 10397–10401.

26 X. Chen, J. Wei, R. Hou, Y. Liang, Z. Xie, Y. Zhu, X. Zhang and H. Wang, Growth of g-C_3N_4 on mesoporous TiO_2 spheres with high photocatalytic activity under visible light irradiation, *Appl. Catal., B*, 2016, **188**, 342–350.

27 W. Zhao, Y. Su, C. Li, Q. Shi, X. Ning and Z. Jiang, Fabrication of antifouling polyethersulfone ultrafiltration membranes using Pluronic F127 as both surface modifier and pore-forming agent, *J. Membr. Sci.*, 2008, **318**, 405–412.

28 X. Li, X. Fang, R. Pang, J. Li, X. Sun, J. Shen, W. Han and L. Wang, Self-assembly of TiO_2 nanoparticles around the pores of PES ultrafiltration membrane for mitigating organic fouling, *J. Membr. Sci.*, 2014, **467**, 226–235.

29 V. Vatanpour, S. S. Madaeni, A. R. Khataee, E. Salehi, S. Zinadini and H. A. Monfared, TiO_2 embedded mixed matrix PES nanocomposite membranes: Influence of different sizes and types of nanoparticles on antifouling and performance, *Desalination*, 2012, **292**, 19–29.

30 J.-H. Li, B.-F. Yan, X.-S. Shao, S.-S. Wang, H.-Y. Tian and Q.-Q. Zhang, Influence of Ag/TiO_2 nanoparticle on the surface hydrophilicity and visible-light response activity of polyvinylidene fluoride membrane, *Appl. Surf. Sci.*, 2015, **324**, 82–89.

31 Y. Zhang, L. Wang and Y. Xu, ZrO_2 solid superacid porous shell/void/TiO_2 core particles (ZVT)/polyvinylidene fluoride (PVDF) composite membranes with anti-fouling performance for sewage treatment, *Chem. Eng. J.*, 2015, **260**, 258–268.

32 Z. Xu, T. Wu, J. Shi, K. Teng, W. Wang, M. Ma, J. Li, X. Qian, C. Li and J. Fan, Photocatalytic antifouling PVDF ultrafiltration membranes based on synergy of graphene oxide and TiO_2 for water treatment, *J. Membr. Sci.*, 2016, **520**, 281–293.

33 R. A. Damodar, S.-J. You and H.-H. Chou, Study the self cleaning, antibacterial and photocatalytic properties of TiO_2 entrapped PVDF membranes, *J. Hazard. Mater.*, 2009, **172**, 1321–1328.

34 B. Lin, C. Xue, X. Yan, G. Yang, G. Yang and B. Yang, Facile fabrication of novel SiO_2/g-C_3N_4 core–shell nanosphere photocatalysts with enhanced visible light activity, *Appl. Surf. Sci.*, 2015, **357**, 346–355.

35 H. Xu, H. Zhao, Y. Song, W. Yan, Y. Xu, H. Li, L. Huang, S. Yin, Y. Li, Q. Zhang and H. Li, g-C_3N_4/Ag_3PO_4 composites with synergistic effect for increased photocatalytic activity under the visible light irradiation, *Mater. Sci. Semicond. Process.*, 2015, **39**, 726–734.